# In-plane force fields and elastic properties of graphene

G. Kalosakas,[1,2] N. N. Lathiotakis,[3] C. Galiotis,[1,2] and K. Papagelis[1,2]

[1]*Materials Science Department, University of Patras, Rio GR-26504, Greece*
[2]*ICE-HT/FORTH, PO Box 1414, GR-26504 Rio, Greece*
[3]*Theoretical and Physical Chemistry Institute, NHRF, Vass. Constantinou 48, Athens GR-11635, Greece*

Bond stretching and angle bending force fields, appropriate to describe in-plane motion of graphene sheets, are derived using first principles' methods. The obtained force fields are fitted by analytical anharmonic energy potential functions, providing efficient means of calculations in molecular mechanics simulations. Numerical results regarding the mechanical behavior of graphene monolayers under various loads, like uniaxial tension, hydrostatic tension, and shear stress, are presented, using both molecular dynamics simulations and first principles' methods. Stress-strain curves and elastic constants, such as, Young modulus, Poisson ratio, bulk modulus, and shear modulus, are calculated. Our results are compared with corresponding theoretical calculations as well as with available experimental estimates. Finally, the effect of the anharmonicity of the extracted potentials on the mechanical properties of graphene are discussed.

## I. INTRODUCTION

Graphene consists of a two-dimensional ($2D$) sheet of covalently bonded carbon and forms the basis of both $1D$ carbon nanotubes, $3D$ graphite but also of important commercial products, such as, polycrystalline carbon (graphite) fibres. As a defect-free material, graphene is predicted to have an intrinsic tensile strength higher than any other known material [1] and tensile stiffness similar to values measured for graphite. Graphene over the years and even prior to its isolation has been an ideal material to model as far as its mechanical properties are concerned. In particular, the elastic moduli of single layer graphene and its elastic response, have been a subject of intensive theoretical research in recent years and quite different approaches have been employed [2–12]. For example, several groups have performed first principles' calculations [6], other used empirical potentials for atomistic simulations [4, 8, 9], and also tight-binding methods have been employed [7, 9]. As it is evident from the literature survey there is a large discrepancy of values regarding the stiffness of monolayer graphene and values ranging from 0.5 $TPa$ to 4 $TPa$ have been proposed depending on the methodology pursued in each case.

From the experimental point of view, recent experiments have indeed confirmed the extreme stiffness of graphene of 1 $TPa$ and provided an indication of the breaking strength of graphene of 42 $N/m$ (or 130 $GPa$ considering the thickness of graphene as 0.335 $nm$) [13]. These experiments involved the simple bending of a tiny flake by an indenter on an AFM set-up and the force-displacement response was approximated by considering graphene as a clamped circular membrane made by an isotropic material. An alternative way to assess how effective graphene is in the uptake of applied stress or strain (uniaxial or biaxial) is to probe the vibrational characteristics of certain interatomic bonds upon loading. In particular, Raman spectroscopy has been proved very successful in monitoring the mechanical response of certain Raman active modes upon the application of external mechanical stress/strain. In axial tension, a linear relationships between Raman frequency and strain was established regardless of the geometry of the monolayer graphene up to strains of about 1.5 % [14–17].

In this work, we present appropriate empirical force fields, derived from first principles' calculations, to describe bond stretching and angle bending interactions in graphene. Analytical nonlinear potentials are provided for these interactions, in order to efficiently implemented in atomistic molecular dynamics or Monte Carlo simulations. A big advantage of atomistic models compared to the more accurate first principles' methods is their computational efficiency which makes them more practical for molecular dynamics simulations especially for finite temperatures. Moreover, when analytical potentials are available, the effect of various types of interactions can be investigated by switching off, or modifying, corresponding potential energy terms, being able to improve in this way our understanding of the studied problem [18]. The obtained empirical potentials are then used to calculate, through molecular dynamics simulations, the mechanical response of graphene under various loads. To test these results, density functional theory calculations of graphene's elastic behavior have been also performed.

The derived bond stretching and angle bending force fields are discussed in the Section II, along with the analytical formulas for the respective potential energies. Then, the Section III contains results concerning the mechanical response of graphene monolayers on uniaxial tension, hydrostatic tension, and shear stress. Stress-strain curves and the corresponding elastic parameters are presented. Finally, the Section IV concludes our work.

## II. IN-PLANE FORCE FIELDS

We performed first principles', Density Functional Theory (DFT) calculations at the GGA/PBE level[19] for an infinite graphene sheet. We used the Quantum-

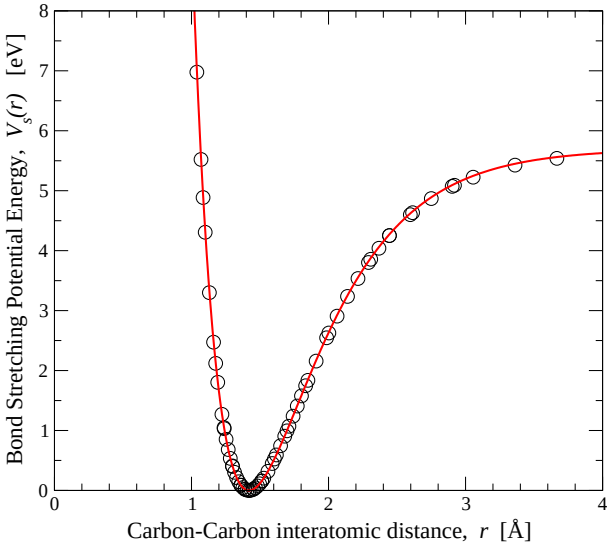


FIG. 1: Bond stretching potential energy as a function of the interatomic distance between bonded carbon atoms in graphene layers. Circles show the results obtained through density functional theory. Solid line represents the best fit with a Morse potential, Eq. (1).

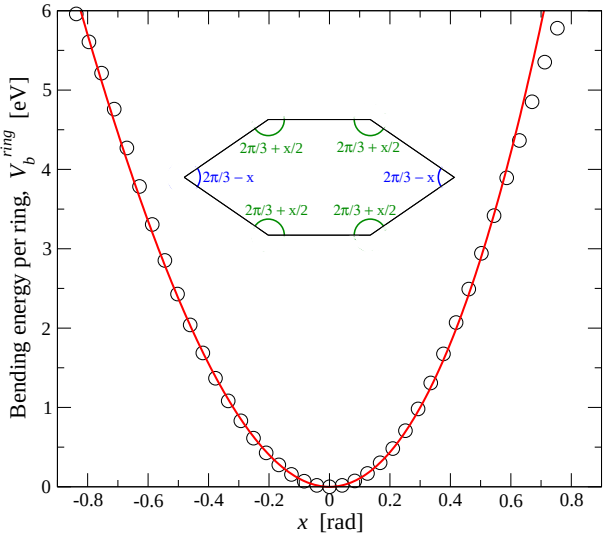


FIG. 2: Bending energy per hexagonal ring as a function of the angle deformation shown in the inset. Circles show the results obtained through density functional theory. Solid line represents the best fit with Eq. (3), from where the parameters of the angle bending potential (2) are derived.

Espresso computer code[20] with a ultra-soft pseudopotential [21] generated by a modified RRKJ approach [22] which is proven to reproduce accurately structural, vibrational and thermodynamic properties of carbon allotropes [23]. Finally, we adopted a minimal two-atom unit cell, a 10×10 k-mesh and cutoffs 70 and 560 Ry for the wave functions and charge density respectively.

To find the energy dependence of the bond stretching motion we scaled the lattice, thus stretching all C-C bonds without altering any valence angle. In Fig. 1 the calculated energy per bond is shown. For efficient atomistic simulations, we have fitted the obtained DFT results with appropriate anharmonic functions, thus providing analytical potentials for the description of the in-plane molecular mechanics of graphene. Regarding bond stretching, the Morse potential

$$V_s(r) = D\left[e^{-a(r-r_0)} - 1\right]^2 \qquad (1)$$

has been considered. Through fitting of the numerical DFT results with eq. (1) , the parameter values $D = 5.7\ eV$, $a = 1.96\ \mathring{A}^{-1}$, $r_0 = 1.42\ \mathring{A}$ have been obtained (see Fig. 1 ).

The angle bending force field is described by a nonlinear potential containing quadratic and cubic terms

$$V_b(\phi) = \frac{k}{2}\left(\phi - \frac{2\pi}{3}\right)^2 - \frac{k'}{3}\left(\phi - \frac{2\pi}{3}\right)^3. \qquad (2)$$

To obtain the parameters $k$ and $k'$ of this expression, we consider the deformed graphene lattice where each benzene ring is identically deformed as shown in the inset of Fig. 2; only the valence angles have been uniformly altered by $x$ or $x/2$, while all bond lengths have their equilibrium value of 1.42 $\mathring{A}$. In the same figure we show the dependence of the DFT calculated total energy per ring on the angle-bending parameter $x$. For such a deformation, considering the angle bending potential energy of Eq. (2), the obtained energy per ring is

$$V_b^{ring} = 2V_b\left(\frac{2\pi}{3} - x\right) + 4V_b\left(\frac{2\pi}{3} + \frac{x}{2}\right) = \frac{3}{2}kx^2 + \frac{1}{2}k'x^3, \qquad (3)$$

Fitting the DFT results of Fig. 2 with the last expression yields the parameter values $k = 7.0\ eV/rad^2$ and $k' = 4\ eV/rad^3$ for the angle bending potential, Eq.(2).

We mention that bond stretching and angle bending potentials like those discussed here, Eqs. (1) and (2), have been also presented in Ref. [24], but with different parameter values: $D = 234.42\ kcal/mol = 10.1\ eV$, $a = 1.75\ \mathring{A}^{-1}$, $r_0 = 1.27\ \mathring{A}$, $k = 36.26\ kcal/mol/rad^2 = 1.56\ eV/rad^2$, and $k' = 0$ (a linear angle bending potential has been considered in that work).

## III. MECHANICAL RESPONSE OF GRAPHENE MONOLAYERS

Stress-strain curves and elastic constants of graphene monolayers have been calculated using both first principle's method and molecular dynamics (MD) atomistic simulations with the potentials presented in the previous section.

In the former case, DFT calculations were performed, as previously, but for a larger rectangular unit cell comprising by 16 atoms and a 6×12 k-mesh. Strains were

applied in one (either the zigzag or armchair, for uniaxial tensions) or both (for hydrostatic tension) of the two vertical directions of the unit cell. For a given strain level the corresponding unit cell dimensions are fixed while all other structural parameters such as atomic positions and vertical to strain unit-cell dimension for uniaxial strain, were allowed to relax. The stresses (forces per length) were calculated as numerical derivatives of the total energy with respect to the appropriate length (or area) of the unit cell for given strain.

In order to obtain the mechanical response of graphene at a fixed force, $f$, acting on one or more of its edges, atomistic simulations have been performed as follows: we start with the equilibrium structure of graphene, without any external force (i.e. all first neighboring distances are 1.42 $\AA$ and all valence angles $2\pi/3$). Then, a constant force $f$ is applied at all atoms of the appropriate edge, depending on the case (the force may be perpendicular or parallel to the edge). Now, the system is out of equilibrium and Newton's equations of motion are numerically solved, applying a friction term at each atom, to follow the evolution of the system. Then, the system gradually goes to a new equilibrium, compatible to the applied forces. In this process, due to the friction the total energy of the system decreases from its initial value towards a new lower value, corresponding to the new equilibrium (the deformed state due to the applied stress). The total kinetic energy increases initially from zero and after some decaying oscillations it gradually vanishes, when the new equilibrium has been reached. During this evolution, strains are developed in the graphene sheet and, following a transient oscillatory behavior, they converge to the equilibrium values corresponding to the applied stress. To avoid finite size effects, the equilibrium strains at the middle of the examined graphene sheets are recorded. Then the same procedure is repeated for another value of the applied force $f$. Graphene monolayers consisting of 7482 and 17030 carbon atoms have been simulated, providing the same results. The friction coefficient was 10 $psec^{-1}$. It has been checked that other values of the friction coefficient result in the same deformed state, affecting only the transient period and the number of oscillations needed before reaching the corresponding equilibrium.

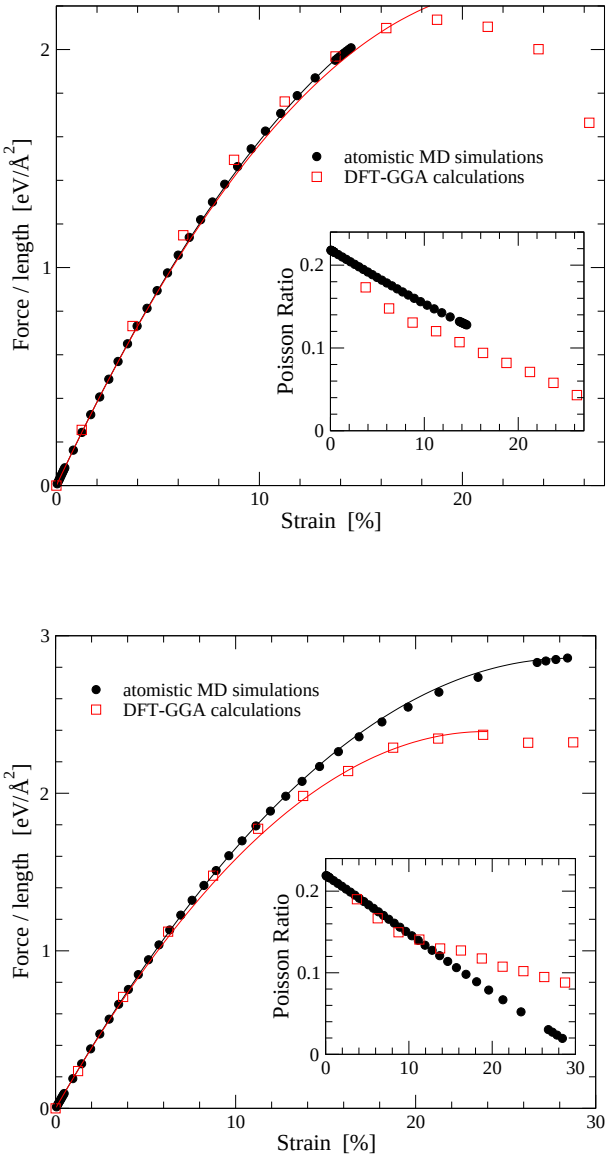


FIG. 3: Stress-strain curves for uniaxial deformations of graphene monolayers. *Top:* The uniaxial tension is applied to graphene's zigzag edges. *Bottom:* The uniaxial tension is applied to graphene's armchair edges. Filled circles show results obtained through molecular dynamics simulations, while open squares correspond to density functional theory calculations. Solid lines represent fits with the nonlinear relation, Eq. (4). The insets depict the variation of the Poisson ratio with the uniaxial strain.

### A. Uniaxial tension

Here, atomistic simulations have been performed, as described above, with a constant force $f$ applied at all atoms belonging to the two opposite edges of graphene. The force is perpendicular to the corresponding edges and it is directed outwards. Fixed strains at the two opposite edges of the unit cell have been imposed in the respective DFT calculations, while the vertical direction has been relaxed to minimize the total energy. For a given strain, the stress is obtained through the numerical derivative of the total energy with respect to the size of the unit cell along the direction where the strains are imposed. MD (DFT) results are presented for the cases where the tensile force (strain) is applied either on the zigzag or on the armchair edges of graphene.

Fig. 3 depicts the force per unit length (the corresponding stress at the edge of a two-dimensional material) as a function of the strain (%) for uniaxial tensions applied on the graphene's zigzag (top) or armchair (bottom) edges. In the former case, the DFT and MD results coincide up

to a strain of 14-15%, above of which failure is obtained in the atomistic simulations. In the latter case, the DFT and MD calculations are almost identical up to about 12-14% strain, while failure is obtained at a strain larger than 28% in the atomistic simulations and a bit earlier in the first principles method.

The slope of the obtained stress-strain curves in the limit of small strains and stresses leads to a $2D$ Young modulus $E_{2D} = 320\ N/m$, for uniaxial tensions applied on both types of graphene edges. Considering the thickness of a graphene monolayer to be $l = 0.335\ nm$ (the interlayer spacing of graphite), the derived effective $3D$ Young modulus is $E_{eff} = E_{2D}/l = 0.96\ TPa$. The $2D$ intrinsic strengths (the maximum tensile stresses supported before failure) are $\sigma^z_{2D} = 32-34\ N/m$ for uniaxial forces applied on the zigzag edges and $\sigma^a_{2D} = 39-45\ N/m$ for uniaxial forces applied on the armchair edges. The effective $3D$ intrinsic strengths, $\sigma_{eff} = \sigma_{2D}/l$, are around 100 $GPa$ and 120-130 $GPa$, respectively. The failure observed in atomistic MD simulations for stresses larger than the intrinsic strength, occurs as shown in Fig. 7 of Ref. [25], i.e. when the tensile force is applied on the armchair (zigzag) edges of graphene, the terminal single layer of atoms on which the forces are applied (the terminal layer of hexagonal atomic rings) breaks and it is disrupted from the system.

The calculated Young modulus and intrinsic strengths are in agreement with available experimental estimates and in the range of theoretically computed values from other works. Early measurements of the elastic constants of highly ordered pyrolytic graphite indicated a value of 1 $TPa$ for the in-plane Young modulus. More recently, indirect experimental estimates, obtained through nanoindentation measurements of free-standing monolayer graphene [13], result in $2D$ Young modulus $E_{2D} = 340 \pm 50\ N/m$ and strength $\sigma_{2D} = 42 \pm 4\ N/m$, leading to effective $3D$ values $E_{eff} = 1.0 \pm 0.1\ TPa$ and $\sigma_{eff} = 130 \pm 20\ GPa$, respectively. Theoretical predictions for the Young modulus of graphene have been obtained through a variety of methods. Molecular mechanics simulations yield $E_{eff} = 0.95\ TPa$ [24], MD simulations $E_{eff} = 1.01\ TPa$ [9], Monte Carlo calculations $E_{eff} = 1.04\ TPa$ ($E_{2D} = 350\ N/m$) [8], tight-binding approximations $E_{eff} = 0.91\ TPa$ [9], and density functional theory methods result in values of $E_{eff} = 1.05 - 1.09\ TPa$ [6, 27, 28]. Intrinsic strengths $\sigma^z_{eff} = 110\ GPa$ and $\sigma^a_{eff} = 121\ GPa$ for forces applied along the zigzag and armchair edges, respectively, have been calculated in Ref. [6].

The elastic response of monolayer graphene under uniaxial extension can be captured by the following nonlinear relation

$$\sigma_{2D} = E_{2D} \cdot \epsilon + D_{2D} \cdot \epsilon^2, \qquad (4)$$

where $\epsilon$ is the uniaxial strain and $D_{2D}$ is the third-order elastic modulus which is typically negative [13]. The Young modulus is about 320 $N/m$ for both directions of uniaxial tension and the $D_{2D}$ is derived through fitting of the numerical data with Eq. (4). When tension is applied on the zigzag edges, the extracted $D_{2D}$ is $-700\ N/m$ in the DFT and $-670\ N/m$ in the MD results. For the armchair direction the obtained $D_{2D}$ values are $-670\ N/m$ and $-560\ N/m$, respectively. These values are in agreement with the experimentally determined value of $-690\ N/m$ [13].

The insets in Fig. 3 show the corresponding Poisson's ratio, $\nu$, as a function of the uniaxial strain. In both directions, a value of $\nu \approx 0.22$ is obtained for small strains, while the Poisson ratio decreases for larger strains. When the uniaxial tension is applied to the zigzag edges, the slope of the almost linear decrease of the Poisson ratio is $-0.006/\%strain$ in both MD and DFT calculations. In the other direction, atomistic simulations give a linear decrease of $\nu$ with a slope of $-0.007/\%strain$, while the DFT calculations coincide with the MD ones for strains up to about 12%, but the slope changes for larger strains resulting in an approximate average slope of $-0.004/\%strain$. Similar behavior has been obtained from the DFT results of Ref. [6], where $\nu$ starts from a value around 0.19 at small strains and then it almost linearly decreases up to strains 25-30%, exhibiting a more abrupt slope in the case of tension applied on the zigzag edges. Other theoretical estimates give values of $\nu$ around 0.15 at 0 $^\circ K$ [8], $\nu = 0.28$ at 1 $atm$ and 300 $^\circ K$ [24], and $\nu = 0.21$ at 300 $^\circ K$ [9].

### B. Hydrostatic tension

In this case, constant forces are applied at all boundary atoms of the graphene sheets studied with MD, in such a way that the corresponding stress (force per unit length) is the same at both kinds of edges. Taking into account that the average interatomic distances *along* the zigzag and armchair edges are $\sqrt{3}r_0/2$ and $0.75r_0$, respectively, the applied forces have different magnitudes at each type of edge. They are perpendicular to the edges and are directed outwards. In the DFT calculations, a uniform strain in both vertical directions was applied. The hydrostatic stress was calculated by numerical differentiation of the energy with respect to the unit cell's area, at given uniform strains. Applying uniform strain in both directions, i.e. assuming that the material is isotropic, is a reasonable approximation as it is justified below.

Fig 4 presents the force per unit length as a function of the relative surface change $DS/S_0 = (S - S_0)/S_0$, where $S_0$ is the initial undeformed surface of the system and $S$ is the final equilibrium surface corresponding to the applied forces. Graphene supports hydrostatic tension up to more than 30% relative change of its surface. The maximum tensile hydrostatic stress before failure is obtained around 31-32 $N/m$, which, divided by $l$, corresponds to an effective $3D$ stress 90-100 $GPa$. This value of maximum stress is close to the intrinsic strength of uniaxial tension applied on the zigzag edge, which is the minimum of the two values of intrinsic strengths corresponding to

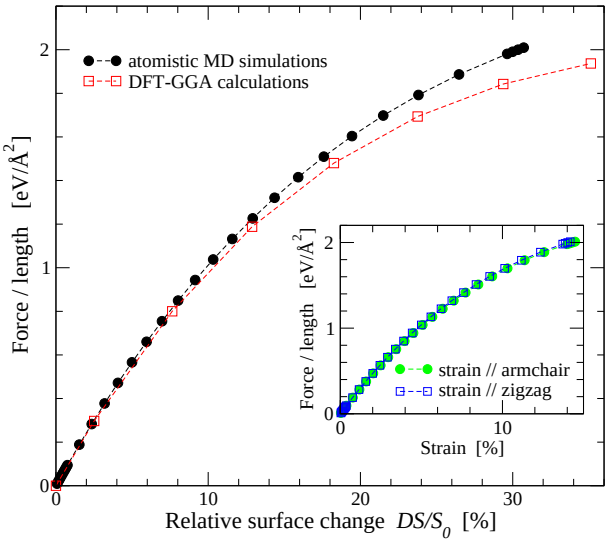


FIG. 4: Stress-strain curve for hydrostatic tension deformation of graphene monolayers. Filled circles (open squares) show results obtained through molecular dynamics simulations (density functional theory calculations). The inset depicts the force per unit length as a function of the relative length deformation along the armchair (filled circles) and the zigzag (open squares) direction, obtained through the molecular dynamics calculations. Dashed lines are guides to the eye.

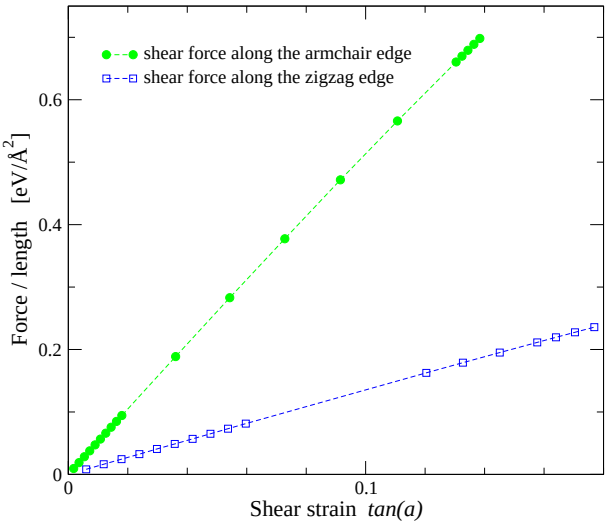


FIG. 5: Stress-strain curves for shear deformations of graphene monolayers, obtained through molecular dynamics simulations. Filled circles (open squares) show results corresponding to shear forces acting on the armchair edge (zigzag edge) of graphene. Dashed lines are guides to the eye.

the two different directions of uniaxial tension. However, this does not imply that hydrostatic failure occurs at the zigzag edges by the same mechanism as in the corresponding uniaxial tension [29]. On the contrary, MD simulations indicate a more complicated failure pattern in this case.

In the small strain/stress limit, the slope of the stress-strain curve shown in Fig 4 results in a $2D$ bulk modulus $B_{2D} = 200\ N/m$. This value of the $2D$ bulk modulus is in agreement with estimates of $B_{2D} \approx 13\ eV/\AA^2 \approx 200\ N/m$, obtained from Monte Carlo simulations [8].

In order to investigate potential asymmetries in the elastic response of graphene under hydrostatic load, we show in the inset of Fig 4 the relation between the applied force per unit length and the relative extensions along the zigzag and armchair directions, separately, as obtained from the atomistic simulations. A completely symmetric response arises, as the strains along the two directions are identical. This confirms the equivalence between the DFT calculations, obtained by applying uniform strains along the two directions, and the hydrostatic MD results, where uniform stresses are applied in the two directions.

### C. Shear stress

Shear deformations are investigated merely by MD simulations.To this end, one edge of graphene has been kept fixed, at its free-of-load equilibrium structure, during the whole MD process, while constant forces are applied at all atoms of the opposite edge. The direction of the forces is parallel to the edge on which they apply. The shear response of both kinds of edges has been calculated through this procedure.

Fig. 5 shows the shear stress as a function of shear strain (the tangent of the strain angle at the middle of the examined graphene sheet). A noticeable asymmetry on the shear response of the zigzag and armchair edges is obtained. The armchair edges can withstand shear stresses up to around 11 $N/m$, where a maximum shear strain 0.14 is developed. A significantly smaller maximum shear stress of less than 4 $N/m$ is supported by the zigzag edges, but with a larger shear strain.

Almost linear stress-strain curves describe the shear deformations of both zigzag and armchair edges of graphene. The obtained $2D$ shear moduli are $G^a_{2D} = 84\ N/m$ for shear stresses applied on the armchair edge and $G^z_{2D} = 22\ N/m$ for shear applied on the zigzag edge. The effective $3D$ shear moduli $G_{eff} = G_{2D}/l$ are 250 $GPa$ and 65 $GPa$, respectively. The asymmetric shear response of the two kinds of edges result in a difference by a factor of about 4 of the corresponding elastic moduli. A higher value of shear modulus in graphene, around 150 $N/m$, has been obtained from Monte Carlo simulations [8].

### D. Effect of the anharmonicity of force fields

As it has been mentioned in the Section I, one of the advantages of atomistic simulations, when analytical force fields are available, is that the influence of several factors can be explored by altering or eliminating respective

potential energy terms. Here, we examine the effect of nonlinear interactions on the uniaxial tensile response of graphene, since both bond stretching and angle bending potentials, Eqs. (1) and (2), presented in this work are anharmonic.

Using respective MD simulations, results have been obtained for the cases that (i) the angle bending potential is linearized by ignoring the cubic term (setting $k' = 0$) in Eq. (2) and (ii) both angle bending and bond stretching potentials are linearized; i.e. additionally to the change mentioned previously, the Morse potential is also linearized through the substitution of Eq. (1) by its harmonic approximation $V_s^{linear} = Da^2(r - r_0)^2$.

Fig. 6 compares the stress-strain curves on uniaxial tension obtained in the cases (i) and (ii) with the corresponding results shown in Fig. 3, where the anharmonic potentials of Eqs. (1) and (2) have been used. The insets present these comparisons regarding the strain dependence of the Poisson ratio. It can be seen that the nonlinearity of the angle bending potential has not any noticeable effect on the calculated mechanical response. Instead, the response is drastically different when harmonic bond stretching potentials are considered too. As expected, in the latter case a linear stress-strain relation is obtained (deviating from the nonlinear response for strains above a few per cent) and no failure is present. Further, the Poisson ratio shows no dependence on the strain, in marked contrast to the behavior observed for nonlinear bond stretching force fields.

## IV. CONCLUSIONS

Empirical bond stretching and angle bending potentials have been presented, suitable for atomistic simulations of graphene. The potentials have been derived using methods from first principles and are expected to accurately represent the respective interactions in graphene. Appropriate nonlinear functions that analytically describe the numerically obtained potentials are provided, for efficient use in molecular mechanics calculations.

The mechanical response of graphene under various loads is examined, through both molecular dynamics simulations, using the calculated empirical force fields, and density functional theory calculations. Stress-strain curves have been presented for uniaxial tensions or shear stresses applied on both armchair and zigzag edges of graphene, as well as for hydrostatic tension. The dependence of Poisson ratio on strain is also calculated in the case of uniaxial tensions. Corresponding elastic moduli, such as Young modulus, two-dimensional bulk modulus, or shear moduli, and maximum values of supported stresses or strain before failure are discussed and compared with experimental estimates, when available, and other theoretical results.

Finally, the effect of the nonlinearity of the potentials on the uniaxial tensile response of graphene is considered. We find that the anharmonicity in the angle bending potential plays no role in the examined mechanical response, but, instead, nonlinear terms of the bond stretching potential crucially affect the obtained elastic behavior and, thus, should be necessarily taken into account.

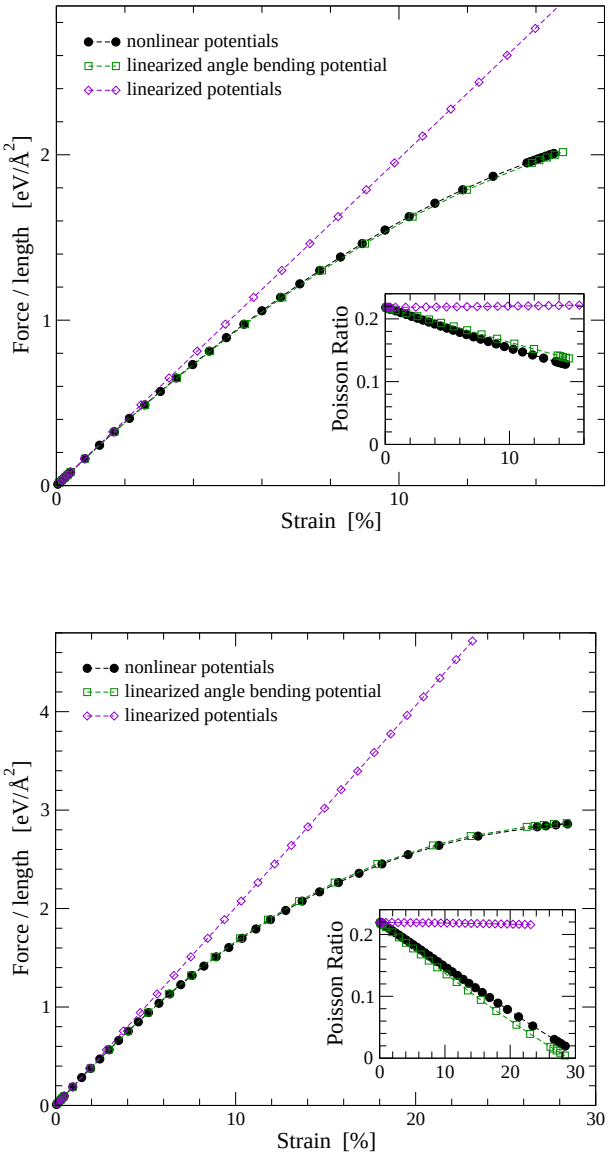


FIG. 6: The effect of the anharmonicity of the potentials on the uniaxial deformations of graphene monolayers. Filled circles show results using the fully nonlinear potentials of Eqs. (1) and (2), open squares correspond to linearized angle bending potential and nonlinear bond stretching potential, while open diamonds correspond to completely linearized potentials. All the results are obtained using molecular dynamics simulations. *Top:* The uniaxial deformation is applied to graphene's zigzag edges. *Bottom:* The uniaxial deformation is applied to graphene's armchair edges. The insets depict the corresponding results for the Poisson ratio as a function of the uniaxial strain. Dashed lines are guides to the eye.

*Acknowledgements* We acknowledge support from the Thales Project GRAPHENECOMP, co-financed by the European Union (ESF) and the Greek Ministry of Edu-

cation (through ΕΣΠΑ program).


[1] Q. Zhao, M.B. Nardelli, J. Bernholc, Phys. Rev. B **65**, 144105 (2002).
[2] K.N. Kudin, G.E. Scuseria, B.I. Yakobson, Phys. Rev. B **64**, 235406 (2001).
[3] G.M. Odegard, T.S. Gates, L.M. Nicholson, K.E. Wise, Compos. Sci. Technol. **62**, 1869 (2002).
[4] Y. Huang, J. Wu, K.C. Hwang, Phys. Rev. B **74**, 245413 (2006).
[5] M. Meo, M. Rossi, Compos. Sci. Technol. **66**, 1597 (2006).
[6] F. Liu, P. Ming, J. Li, Phys. Rev. B **76**, 064120 (2007).
[7] E. Cadelano, P.L. Palla, S. Giordano, L. Colombo, Phys. Rev. Lett. **102**, 235502 (2009).
[8] K.V. Zakharchenko, M.I. Katsnelson, A. Fasolino, Phys. Rev. Lett. **102**, 046808 (2009).
[9] H. Zhao, K. Min, N.R. Aluru, Nano Lett. **9**, 3012 (2009).
[10] A.Sakhaee-Pour, Solid State Communications **149**, 91 (2009).
[11] Z. Ni, H. Bu, M. Zou, H. Yi, K. Bi, Y. Chen, Physica B **405**, 1301 (2010).
[12] J.-L. Tsai, J.-F. Tu, Materials and Design **31**, 194 (2010).
[13] C. Lee, X. Wei, J.W. Kysar, J. Hone, Science **321**, 385 (2008).
[14] G. Tsoukleri, J. Parthenios, K. Papagelis, R. Jalil, A.C. Ferrari, A.K. Geim, K.S. Novoselov, C. Galiotis, Small **21**, 2397 (2009).
[15] O. Frank, G. Tsoukleri, I. Riaz, K. Papagelis, J. Parthenios, A.C. Ferrari, A.K. Geim, K.S. Novoselov, C. Galiotis, Nature Communications 2:255 doi: 10.1038/ncomms1247 (2011).
[16] J. Zabel, R.R. Nair, A. Ott, T. Georgiou, A.K. Geim, K.S. Novoselov, C. Casiraghi, Nano Lett. **12**, 617 (2011).
[17] O. Frank, M. Bouoa, I. Riaz, R. Jalil, K.S. Novoselov, G. Tsoukleri, J. Parthenios, L. Kavan, K. Papagelis, C. Galiotis, Nano Lett. **12**, 687 (2012).
[18] G. Kalosakas, K.L. Ngai, S. Flach, Phys. Rev. E **71**, 061901 (2005).
[19] J.P. Perdew, K. Burke, M. Ernzerhof, Phys. Rev. Lett. **77**, 3865 (1996).
[20] P. Giannozzi, S. Baroni *et al.*, J. Phys.: Cond. Matt. **21**, 395502 (2009).
[21] A. Dal Corso, C.pbe-rrkjus.upf, http://www.quantum-espresso.org/wp-content/uploads/upf_files/C.p
[22] A.M. Rappe, K.M. Rabe, E. Kaxiras, J.D. Joannopoulos, Phys. Rev. B **41**, R1227 (1990).
[23] N. Mounet, N. Marzari, Phys. Rev. B **71**, 205214 (2005).
[24] D. Wei, Y. Song, F. Wang, J. Chem. Phys. **134**, 184704 (2011).
[25] Y. Gao, P. Hao, Physica E **41**, 1561 (2009).
[26] O.L. Blakslee, D.G. Proctor, E.J. Seldin, G.B. Spence, T. Weng, J. Appl. Phys. **41**, 3373 (1970).
[27] C.D. Zeinalipour-Yazdi, C. Christofides, J. Appl. Phys. **106**, 054318 (2009).
[28] P. Wagner, C.P. Ewels, V.V. Ivanovskaya, P.R. Briddon, A. Pateau, B. Humbert, Phys. Rev. B **84**, 134110 (2011).
[29] C.A. Marianetti, H.G. Yevick, Phys. Rev. Lett. **105**, 245502 (2010).